Deng *et al. Journal of Nanobiotechnology* (2025) 23:427
https://doi.org/10.1186/s12951-025-03499-4

Journal of Nanobiotechnology

RESEARCH Open Access

The effects of Klotho delivering mesenchymal stem cell-derived small extracellular vesicles on acute kidney injury

Xiao-Hui Deng[1,2,3,4†], Zi-Cong Wu[1,2,4†], Qi Sun[1], Long-Xin Huang[1], Ying-Chun Xie[1], Dong-Xiao Lou[1], Chan-Gu Li[1], Xiao-Qing Liu[1], Zhi-Rou Zhou[1], Tian Tian[1], Chang-Lin Lian[2,4] and Qing-Ling Fu[1,2,4*]

Abstract

Acute kidney injury (AKI) is a life-threating syndrome characterized by sudden loss of kidney function, and its management is challenging and often suboptimal. Mesenchymal stem cells (MSCs) have shown promise in AKI therapy in pre-clinical and clinical trials; however, their clinical application still faces many challenges. MSC-derived small extracellular vesicles (sEV) may help overcome these challenges. In the current study, we overexpressed Klotho in MSCs and then isolated Klotho-loaded sEV (Klotho-sEV) using anion-exchange chromatography. Klotho-sEV displayed characteristics comparable to those of sEV in terms of size, morphology, conventional markers, and biosafety, as well as a higher abundance of Klotho protein. In rhabdomyolysis-induced AKI, sEV showed preferential tropism in injured kidneys. We found significantly and stably accelerated renal recovery, mitigated functional and histological abnormalities, stimulated tubular cell proliferation, reduced injury and inflammatory marker expression, and restored endogenous Klotho loss in mice after the administration of Klotho-sEV. In addition, Klotho-sEV treatment activated the mTOR and MEK1/2 signaling pathways. Proteomics and small RNA sequencing analyses of sEV and Klotho-sEV revealed abundant proteins and miRNAs involved in anti-inflammation and reno-protection, and Klotho-sEV showed characteristics that were different from those of sEV. In conclusion, Klotho-sEV may be a promising cell-free strategy for the treatment of AKI.

†Xiao-Hui Deng and Zi-Cong Wu contributed equally to this work and share first authorship.

*Correspondence:
Qing-Ling Fu
fuqingl@mail.sysu.edu.cn

Full list of author information is available at the end of the article

Graphical abstract

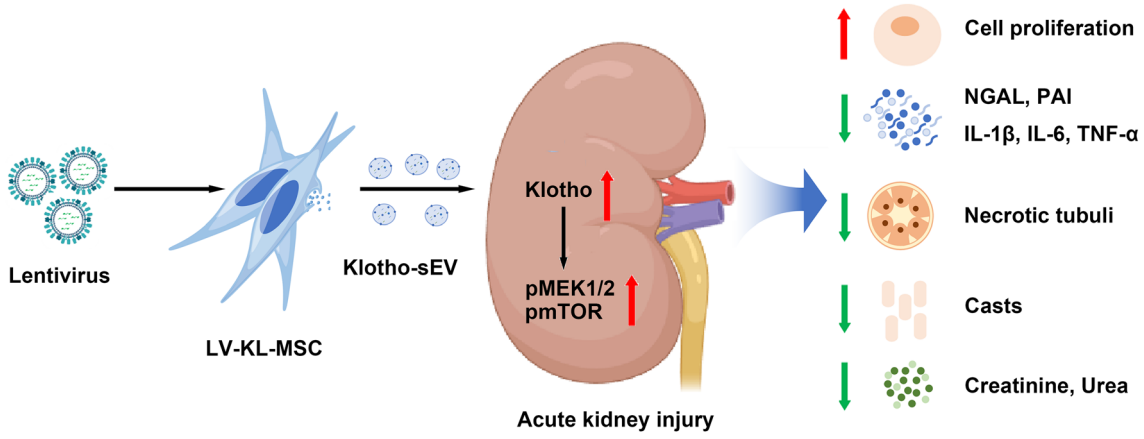

Keywords Mesenchymal stem cells, Small extracellular vesicles, Klotho, Acute kidney injury, Reno-protection

Introduction

Acute kidney injury (AKI) is characterized by a sudden loss of renal function and strongly associated with high morbidity and mortality [1, 2]. It is a common complication in hospitalized patients, and the pooled world incidence and associated mortality rates of AKI are 21.6% and 23.9%, respectively, during a hospital episode of care [3], while its incidence in intensive care has been reported in more than 50% of patients [4]. AKI management in critical care settings, which includes providing optimal nutritional support, nephrotoxic drug management, appropriate volume control, and timing and type of kidney support, is challenging. The management of AKI is often suboptimal. Therefore, improvement of AKI treatment is an urgent and unmet medical need.

Stem cell-based treatments have proven to be promising for AKI owing to their physiological activities related to immunomodulation, apoptosis, angiogenesis, and tissue regeneration in extensive pre-clinical and clinical studies [5–7]. It is worth noting that mesenchymal stem/stromal cells (MSCs) have been widely documented therapeutic efficacy in many pre-clinical models and a record safety in human beings. Although MSCs have these advantages, defects in immunogenicity, stability, storage, and transportation restrict their clinical application [8–10].

Nowadays, increasing and compelling evidence suggests that MSCs can exert their paracrine effects by releasing extracellular vesicles (EV), a class of roughly 50–1000 nm nanometer-sized particles with a lipid membrane enclosure. EV are secreted by all the cell types [11]. In particular, small extracellular vesicles (sEV, within 200 nm in diameter) carrying proteins, nucleic acids, and lipid cargo propagate the key immunoregulatory and regenerative characteristics of their parental cells and have been reported to exert therapeutic effects in many pre-clinical studies [12–16]. Unlike its parental cells, MSC-derived sEV have remarkable advantages including, but not limited to, low immunogenicity, no oncogenicity, good biocompatibility, no cell structure, convenience of storage and transportation, and acting as drug carriers. By transferring the biological cargo of MSCs to recipient cells, sEV may act through multiple regenerative processes, including the inhibition of inflammation, promotion of tubular cell survival and proliferation, and suppression of fibrosis, in AKI [17–19].

Moreover, the lipid biolayer membrane structure of sEV not only makes them convenient for drug carriage but also protects the cargo from degeneration. Klotho, a single-pass transmembrane protein that plays a vital role in renal tissue regeneration, is insufficient in MSC-sEV [20]. Klotho, initially known as an anti-aging gene, is highly expressed in the kidneys [21, 22]. There are two forms of Klotho protein (a membrane form and a secreted form), the extracellular domain of which is cleaved by membrane-anchored proteases and released into circulation. Both forms demonstrate biologic effects [23]. Results from existing literature have shown that Klotho is closely associated with acute and chronic kidney damage, and exogenous Klotho supplementation can be a promising approach for AKI therapy [24–26].

In this study, we aimed to construct Klotho-loaded MSC-sEV (Klotho-sEV) to combine the reno-protective and pro-regenerative effects of Klotho and sEV. We also explored the therapeutic effects of Klotho-sEV on rhabdomyolysis-induced AKI, and identified functional proteins and nucleic acids that may have a synergistic therapeutic effect on AKI.

Materials & methods

Generation of Klotho-overexpressed MSCs

The preparation of human induced-pluripotent stem cell (iPSC)-derived MSCs and purification of sEV have been described previously [27]. Klotho was overexpressed in cultured MSCs and loaded into MSC-derived sEV. Briefly, recombinant lentiviruses of LV-EF1a-3XFlag-Klotho-P2A-EGFP-PGK-Puro-WPRE (plasmid information is shown in Supplementary Fig. 1) and LV-EF1a-3XFlag-P2A-EGFP-PGK-Puro-WPRE were designed and constructed by the Brain VTA. MSCs were seeded at 2×10^5 cells/well in 6-well plates. When MSCs reached 40–50% confluence, LV-EF1a-3XFlag-Klotho-P2A-EGFP-PGK-Puro-WPRE or LV-EF1a-3XFlag-P2A-EGFP-PGK-Puro-WPRE (MOI = 50) was added to the culture medium, which was replaced with a fresh culture medium 24 h later. To select Puromycin-resistance cells, 2 μg/mL Puromycin (InvivoGen, ant-pr-1) was used. Viral infection and selection were performed twice. Flow cytometry analysis revealed that 74% of MSCs were green fluorescent protein (GFP)-positive.

Isolation of sEV using anion-exchange chromatography

Klotho-overexpressed MSCs were further passaged and seeded in 150 cm^2 cell culture plates. When the cells reached 80–90% confluency, the medium was replaced with chemically defined and protein-free medium (CDPF). Six h later, the medium was discarded and replaced with fresh CDPF medium for another 42 h of incubation. After 42 h of incubation, CDPF were collected for the isolation of sEV using anion-exchange chromatography. Briefly, an Econo-Pac column (Bio-Rad Laboratories, CD63 Hercules, CA, USA) with 4 mL of equilibration buffer was packed with 4 mL of anion-exchange resin (Q Sepharose Fast Flow; GE Healthcare Life Science, Pittsburgh, PA, USA) and equilibrated with another 8 mL of equilibration buffer. Then, 150 mL of CDPF was loaded into the column, followed by 40 mL of wash buffer to remove proteomic impurities, and the sEV were eluted by 1 mL elution buffer for eight times. The sEV concentrations were estimated using the Bradford protein assay. The fractions with peak concentration of sEV were pooled for PBS dialysis overnight at 4 °C. An ultrafiltration device (30 kDa; Thermo Fisher Scientific, San Jose, CA) was used to concentrate the sEV [27]. The final concentration of the sEV was determined using the Bradford protein assay. The isolated sEV were either used for study immediately or preserved at − 80 °C.

Nanoparticle tracking analysis

The particle size of the sEV was determined using nanoparticle tracking analysis (Nanosight NS300, Malvern). The samples were diluted to 1:100 or 1:200 in particle-free PBS before analysis. Each sample was recorded for three 30 s videos.

Transmission electron microscopy for sEV

Fresh sEV samples were fixed in 2% glutaraldehyde (Sigma-Aldrich) for 30 min. Next, 10 μL of fixed samples were incubated with copper grids with carbon-coated formvar film for 10 min. Then, the grids were incubated with 30 μL of 3% uranyl acetate (Sigma-Aldrich) for 5 min after three washes with H_2O. The sEV were photographed using a Tecnai G2 SpiritTwin + GATAN 832.10 W instrument (FEI).

Western blot analysis

The protein levels of sEV and cell lysates were quantified using the Pierce™ BCA protein assay (Thermo Fisher Scientific, San Jose, CA), and then equal amount of protein was denatured in SDS loading buffer at 95 ℃ for 10 min. Then, 10–30 μg of the samples were loaded, separated by SDS-PAGE and transferred to polyvinylidene difluoride membranes (Roche Diagnostics, Mannheim). The membranes were blocked with 5% skimmed milk for 1–2 h and further incubated with antibody CD9 (1:2000, ab263019), CD63 (1:2000, ab134045), CD81 (1:2000, ab109201), Alix (1:5000, ab186429), TSG101 (1:1000, ab125011), Calnexin (1:1000, ab133615), GM130 (1:1000, ab52649), Klotho (1:1000, ab181373), AKT (1:1000, 9272 S), pAKT (1:1000, 4060 S), pmTOR (1:1000, 5536T), MEK1/2 (1:1000, 8727 S), pMEK1/2 (1:1000, 9154), GAPDH (1:2000, 5174T) at 4 °C overnight. After three washes with TBST (10 min), the membranes were incubated with HRP-conjugated Goat Anti-Rabbit IgG (1:1000–2500, cw0103s) for 1–2 h. The membranes were washed three times with TBST (10 min), incubated with Enhanced Chemiluminescence Plus (Millipore Corporation), and photographed using an imaging analysis system (ChemiDoc Touch, Bio-RAD). The primary antibodies were purchased from Abcam (Cambridge, UK) and Cell Signaling Technology (Danvers, Massachusetts, USA).

NanoFCM

The location of Klotho was determined using a NanoFCM (NanoFCMU30). Briefly, Klotho-sEV were treated with 0.1% Triton X-100 (ELR00280, eLGbio) (diluted by PBS) or equal volume of PBS at 37 ℃ for 30 min. The Klotho-sEV were washed with PBS and concentrated using an ultrafiltration device. Next, Klotho-sEV were incubated with antibody Klotho (1:50, ab181373) at 4 ℃ for 30 min. After wash and concentration, Klotho-sEV were incubated with Goat Anti-Rabbit IgG H&L (Alexa Fluor® 647) (1:1000, ab150083) at 37 ℃ for 30 min. After another wash and concentration, the Klotho-sEV were recorded

using NanoFCM. The antibodies were purchased from Abcam (Cambridge, UK).

Enzyme-linked immunosorbent assay (ELISA)

Klotho levels in the Klotho-sEV and sEV were determined using the Human Klotho ELISA Kit (SEKH-0221, Solarbio). All procedures were performed according to the manufacturer's instructions.

The uptake effects of human proximal tubular (HK2) cells on sEV

The HK2 cells were a gift from Professor Yi Zhou (The First Affiliated Hospital, Sun Yat-sen University). To determine the uptake effects of HK2 cells on sEV, they were co-cultured with 20 μg/mL mCherry-labelled sEV for 3 h, 6 h, 9 h, 12 h, 24 h, 48 h and 72 h, and the mean fluorescence intensity (MFI) of mCherry in HK2 cells was analyzed using flow cytometry. The HK2 cells were co-cultured with 20 μg/mL mCherry-labelled sEV for 24 h and the nuclei were counterstained using 4′, 6-diamidino-2-phenylindole (DAPI, Invitrogen). The HK2 cells were then photographed using an Olympus BX63 microscope (BX63).

Model of myoglobin-induced cytotoxicity

Based on the existing literature [28, 29] and our pilot study, a concentration of 4 mg/mL (240 μM) ferrous myoglobin was applied in this study. A mixture of 240 μM Myoglobin (M0630, Sigma-Aldrich) and 2.4 mM ascorbic acid (A4544, Sigma-Aldrich) was prepared to obtain the ferrous myoglobin media. Prior to ferrous myoglobin treatment, the HK2 cells were co-cultured with 25 μg/mL sEV for 24 h. After 20–24 h of exposure to ferrous myoglobin, the HK2 cells were analyzed.

Animals

Female C57BL/6 mice aged 4–6 weeks were purchased from GemPharmatech Co., Ltd. The animals were maintained in a specific pathogen-free environment at the Animal Experimental Center of the North Campus, Sun Yat-sen University. All animal procedures were approved by the Ethics Committee of Sun Yat-sen University (SYSU-IACUC-2022-000827).

Rhabdomyolysis-induced AKI

Based on the existing literature [30–33] and our pilot study, AKI was induced in 8-week-old C57BL/6 mice with 18–24 h of water deprivation by intramuscular injection of 8 mL/kg of a 50% hypertonic glycerol solution (Sigma-Aldrich) into the inferior hind limbs. On Day 1, post injury, the mice received a tail vein injection of 500 μg/mL sEV/Klotho-sEV in 200 μL saline (sEV/Klotho-sEV group) or the same volume of PBS (Vehicle group). The mice were sacrificed 48 h after sEV administration. Serum creatinine and urea were measured. For renal histology, paraffin-embedded kidney sections were routinely stained with hematoxylin and eosin (HE) and Periodic Acid-Schiff (PAS). The number of casts and tubular profiles showing necrosis was assessed in non-overlapping fields (up to 10 for each section) using a 20× objective. The number of proliferating cell nuclear antigen (PCNA)-positive cells was evaluated by counting the number of positive nuclei per field in 10 randomly chosen Sect. (20× magnification) using ImageJ software.

Biosafety assessment

As shown in Fig. 10A, healthy mice received a tail vein injection of 500 μg/mL sEV/Klotho-sEV in 200 μL saline (sEV/Klotho-sEV group) or the same volume of PBS (Control group) on Day 0 and 1, respectively. The body weights were recorded every other day for two weeks. Then, the mice were sacrificed. Serum creatinine and urea were measured. For renal histology, paraffin-embedded kidney sections were routinely stained with HE.

Quantitative real-time PCR (RT-PCR)

Total RNA was extracted using RNAiso Plus (TAKARA, 9109). Isolated RNA was used for synthetization of cDNA templates using PrimeScript™ RT Master Mix (Perfect Real Time) (TAKARA, RR036A). Quantitative real-time PCR was performed using the FastStart Universal SYBR Green Master (Rox) (Roche, 4913914001) on Applied Biosystems QuantStudio™ 5 System (Thermo Fisher Scientific, San Jose, CA).

Primer information:

Primer	F	*R*
Hu-beta-actin	CTCCATCCTGGCCTCGCTGT	GCTGTCACCTTCACCGTTCC
Mu-beta-actin	CGTGCGTGACATCAAAGAGAAG	CGTTGCCAATAGTGATGACCTG
Hu-Klotho	GCGTCCATCTGGGATACGTT	TCGCGGAAGACGTTGTTGTA
Mu-IL-6	ACCAGAGGAAATTTTCAATAGGC	TGATGCACTTGCAGAAAACA
Mu-IL-1β	CAACCAACAAGTGATATTCTCCATG	GATCCACACTCTCCAGCTGCA
Mu-TNF-α	CATCTTCTCAAAATTCGAGTGACAA	TGGGAGTAGACAAGGTACAACCC
Mu-PAI	AGTCAATGAGAAGGGCACAGCT	TAGGTCCCGCTGGACAAAGAT
Mu-SOX9	AGTACCCGCATCTGCACAAC	ACGAAGGGTCTCTTCTCGCT
Mu-NGAL	TGCACAGGTATCCTCAGGTACAGA	GGAAAAATACCATGGCGAACTG

Cytometry

For analyses of MSC surface markers, anti-HLA-DR-APC/Cyanine7 (Biolegend, 307617), anti-CD14-PE-CYN7 (eBioscience, 25-0149-42), anti-CD73-APC (Biolegend, 344005), anti-CD105-APC (Biolegend, 800507), anti-CD90-APC (Biolegend, B322310), anti-CD34-PE (Biolegend, 4341649), anti-CD45-APC (BD, 560973), and anti-CD19-PerCP-Cyanine5.5 (eBioscience, 45-0198-41) were used.

For apoptotic cell analysis, an Annexin V/PI Apoptosis Detection Kit (Yeasen, 40302ES60) was used according to the manufacturer's instructions.

sEV biodistribution

NanoLuc-MSC were prepared similarly to LV-KL-MSC, and the isolated sEV were called NanoLuc-sEV. For sEV tropism detection, the mice were subjected to rhabdomyolysis-induced AKI. After 3 d post-administration, the mice were administrated intravenously with 150 μg sEV or NanoLuc-sEV for 1 h, the main organs were surgically exposed, collected, and subjected to Nano-Glo Luciferase Assay (1:400 dilution in PBS) for 1–2 min for further detection of luminescence intensity on the IVIS Spectrum system.

Proteomic analysis of kidneys

Four-dimensional data-independent acquisition (4D-DIA) proteomics was performed by Metware Biotechnology Co., Ltd. Briefly, kidney tissues were used for protein extraction, and the total protein concentration was measured using the BCA protein quantitation assay. Equal amounts of protein from each sample were used for tryptic digestion. Liquid chromatography was performed on a nanoElute UHPLC (Bruker Daltonics, Germany). The liquid chromatography was coupled online to a hybrid timsTOF Pro2 (Bruker Daltonics, Germany) via a Captive Spraynanoelectrospray ion source (CSI). ['DIA-NN(v1.8.1)'] with library-free method was used to analyze the raw MS data. The Homo sapiens SwissProt database (20425 entries) was used to create a spectral library using deep-learning algorithms for neural networks. The MBR was employed to create a spectral library from the DIA data, which was then reanalyzed. The FDR of the search results was adjusted to < 1% at both the protein and precursor ion levels, and the remaining identifications were used for further quantification analysis. Fold change (Fc) > 1.5 or < 0.6667 and p value < 0.05 was set as significant.

Proteomic analysis of sEV and Klotho-sEV

Isobaric tags for relative and absolute quantification (iTRAQ) proteomics were performed by BGI Co., Ltd. After protein extraction, quality control, and proteolysis, the peptide samples were dissolved in 0.5 M TEAB and added to the corresponding iTRAQ labelling reagent (different sample peptides used different iTRAQ labels). The Shimadzu LC-20AB liquid phase system was used, and the separation column was a 5 μm 4.6 × 250 mm Gemini C18 column for liquid phase separation of the sample. The separation was performed using a Thermo UltiMate 3000 UHPLC system. The peptides separated using liquid-phase chromatography were ionized using a nanoESI source and passed to a Q-Exactive HF X tandem mass spectrometer (Thermo Fisher Scientific, San Jose, CA) for data-dependent acquisition (DDA) mode detection. Quantitative analysis of the labelled peptides with isobaric tags was performed using the automated software IQuant. The differentially expressed proteins (DEPs) were defined by their q value ≤ 0.05 and |log2Fc| ≥ 0.26303.

Small RNA sequencing of sEV and Klotho-sEV

Small-RNA sequencing was performed by BGI Co., Ltd. The parameters for calculating the significant differential expression of DEseq2 are |log2Fc| > 0 & q value ≤ 0.05, and the parameters for calculating the significant differential expression of DEGseq and PossionDis are |log2Fc| ≥ 1 & q value ≤ 0.001.

Statistical analysis

Statistical analysis was performed using the Prism software (GraphPad Software). The statistical analysis was assessed using the unpaired Student's t-test for single comparisons or one-way ANOVA with Tukey's or Dunnett's correction for multiple comparisons. A P-value less than 0.05 was considered statistically significant.

Results

Engineering and characterization of Klotho-overexpression MSCs

The Klotho expression was insufficient in MSC-derived sEV (0.19 μg in 100 μg sEV). To load Klotho into sEV, we first designed and constructed a recombinant lentivirus, then cultured human iPSC-derived MSCs transfected with the recombinant lentivirus of LV-EF1a-3XFlag-Klotho-P2A-EGFP-PGK-Puro-WPRE (LV-KL-MSC) or LV-EF1a-3XFlag-P2A-EGFP-PGK-Puro-WPRE (LV-MSC) (Fig. 1A). The MSCs infected with lentiviruses were GFP-positive (Fig. 1B). We found that the frequencies of GFP^+ MSCs were 74% (Fig. 1C) and the mRNA levels of Klotho were significantly increased in LV-KL-MSC (Fig. 1D). Western blot results showed that Klotho protein was overexpressed in MSCs (Fig. 1E). In addition, we found that Klotho overexpression did not affect the expression of MSC markers, including positive (CD73, CD90, and CD105) and negative (CD14, CD19, CD34, CD45, and HLA-DR) markers [34, 35] (Fig. 1F). Therefore, we successfully built a steady cell line by transfecting

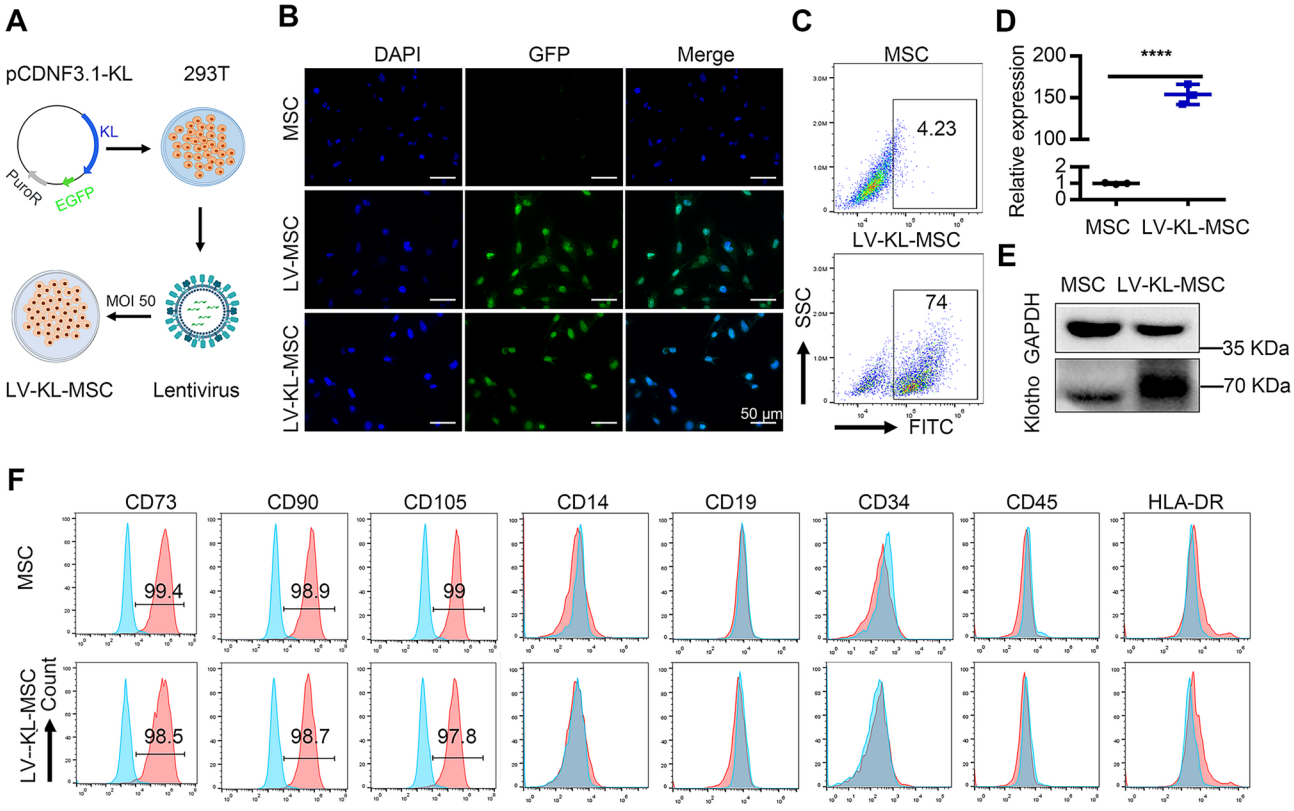

Fig. 1 Klotho-overexpressed mesenchymal stem cell preparation. (**A**) Schematic diagram for the preparation of Klotho-overexpressed MSCs. (**B**) Detection of green fluorescent protein (GFP) in purified MSCs by means of fluorescent microscopy. Original magnification ×400. (**C**) Flow cytometry analyses showed that 74% MSCs were GFP (FITC) positive. (**D**) mRNA levels of Klotho were determined using quantitative real-time PCR (RT-PCR). (**E**) Klotho protein was overexpressed in MSCs as determined using western blot. (**F**) Flow cytometry analyses showed that the overexpression of Klotho could not change MSC maker expression (Red, MSCs labelled with antibody; Blue, blank). In all plots, mean with SD are shown. ****$p < 0.0001$ by unpaired t-test

MSCs with a lentivirus to achieve overexpression of Klotho.

Isolation and characterization of Klotho-sEV

We isolated sEV from the cell culture CDPF medium using anion-exchange chromatography (Fig. 2A). As determined by nanoparticle tracking analysis, the mean diameters of sEV (163.5 nm) and klotho-sEV (166.7 nm) were comparable, both with a sharp peak at approximately 150 nm diameter (Fig. 2B). sEV/Klotho-sEV with a diameter of less than 200 nm were confirmed by transmission electron microscopy, which revealed the characteristic lipid bilayer (Fig. 2C). Using western blot, we further confirmed that sEV and Klotho-sEV were positive for the conventional sEV markers CD9, CD63, CD81, ALIX, and TSG101, and negative for Calnexin and GM130 (Fig. 2D). As expected, the Klotho protein was successfully loaded into the sEV (Fig. 2E). We further confirmed that Klotho was mostly located on the membrane of the sEV using NanoFCM (Fig. 2F). The levels of Klotho in Klotho-sEV were further analyzed using ELISA, and we identified that the levels of Klotho were 2.15 μg in 100 μg Klotho-sEV. In summary, encapsulation of Klotho in sEV did not affect their characteristics in terms of size, morphology, and conventional markers.

Klotho-sEV ameliorated rhabdomyolysis-induced AKI

Myoglobin plays a vital role in rhabdomyolysis-induced AKI [28, 29, 36]. To explore the effects of Klotho-sEV on myoglobin-induced cell apoptosis, we successfully developed an in-vitro cell model using 4 mg/mL ferrous myoglobin. Klotho-sEV pre-treatment stably ameliorated myoglobin-induced tubular cell apoptosis, and increased live cell frequencies (Supplementary Fig. 2). Collectively, these data revealed that Klotho-sEV attenuate myoglobin-induced apoptosis in HK2 cells.

To further explore the potential effects of Klotho-sEV on rhabdomyolysis-induced AKI, we developed a murine model by intramuscular injection of 8 mL/kg of a 50% hypertonic glycerol solution into the inferior hind limbs (Fig. 3A). Creatinine and urea are recognized kidney function biomarkers. We found that the intramuscular injection of hypertonic glycerol sharply increased the levels of creatinine and urea in the blood, revealing that the model was successfully developed. Mice injected with Klotho-sEV showed a notable reduction in creatinine

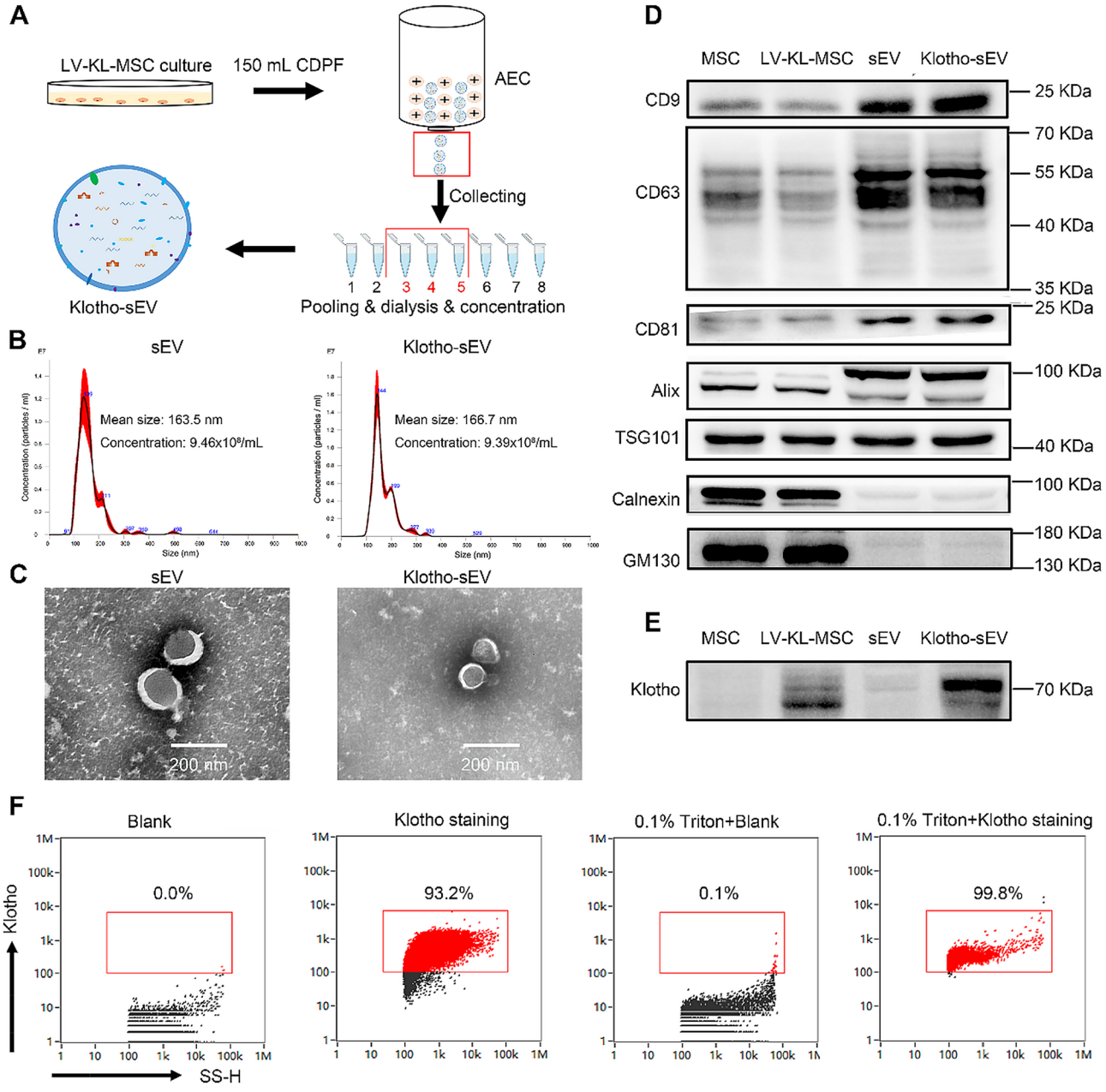

Fig. 2 The characterization of Klotho-sEV. (**A**) Schematic diagram of the isolation of small extracellular vesicles (sEV)/Klotho-sEV using anion-exchange chromatography (AEC). (**B**) Representative results of the sEV/Klotho-sEV nanoparticle tracking analyses. (**C**) Transmission electron microscopy images of sEV/Klotho-sEV (scale bar, 200 nm). Original magnification ×59,000. (**D**) sEV/Klotho-sEV were positive for CD9, CD63, CD81, and ALIX and negative for Calnexin and GM130, as determined using western blotting. (**E**) Klotho protein levels in sEV/Klotho-sEV were determined using western blotting. (**F**) Klotho localization was determined using NanoFCM

and urea levels on Day 3, whereas the effects of sEV seemed unstable (Fig. 3B and C). To further confirm the effects of Klotho-sEV on AKI, the kidney sections were histologically evaluated. Histological evaluation of the vehicle group revealed casts and necrosis of the tubular epithelial cells. Compared with the vehicle group, mice that received Klotho-sEV treatment showed a significantly decreased number of casts and necrotic tubules. No significant difference was observed between the sEV treatment and vehicle groups, as determined by HE staining (Fig. 3D). This was confirmed by PAS staining (Fig. 3E).

The regenerative effects of Klotho-sEV were confirmed using PCNA staining. Compared with PBS and sEV treatments, Klotho-sEV treatment promoted renal cell proliferation (Fig. 4A). We further analyzed the effects of Klotho-sEV on renal damage and inflammatory markers at the mRNA level. In particular, AKI mice showed

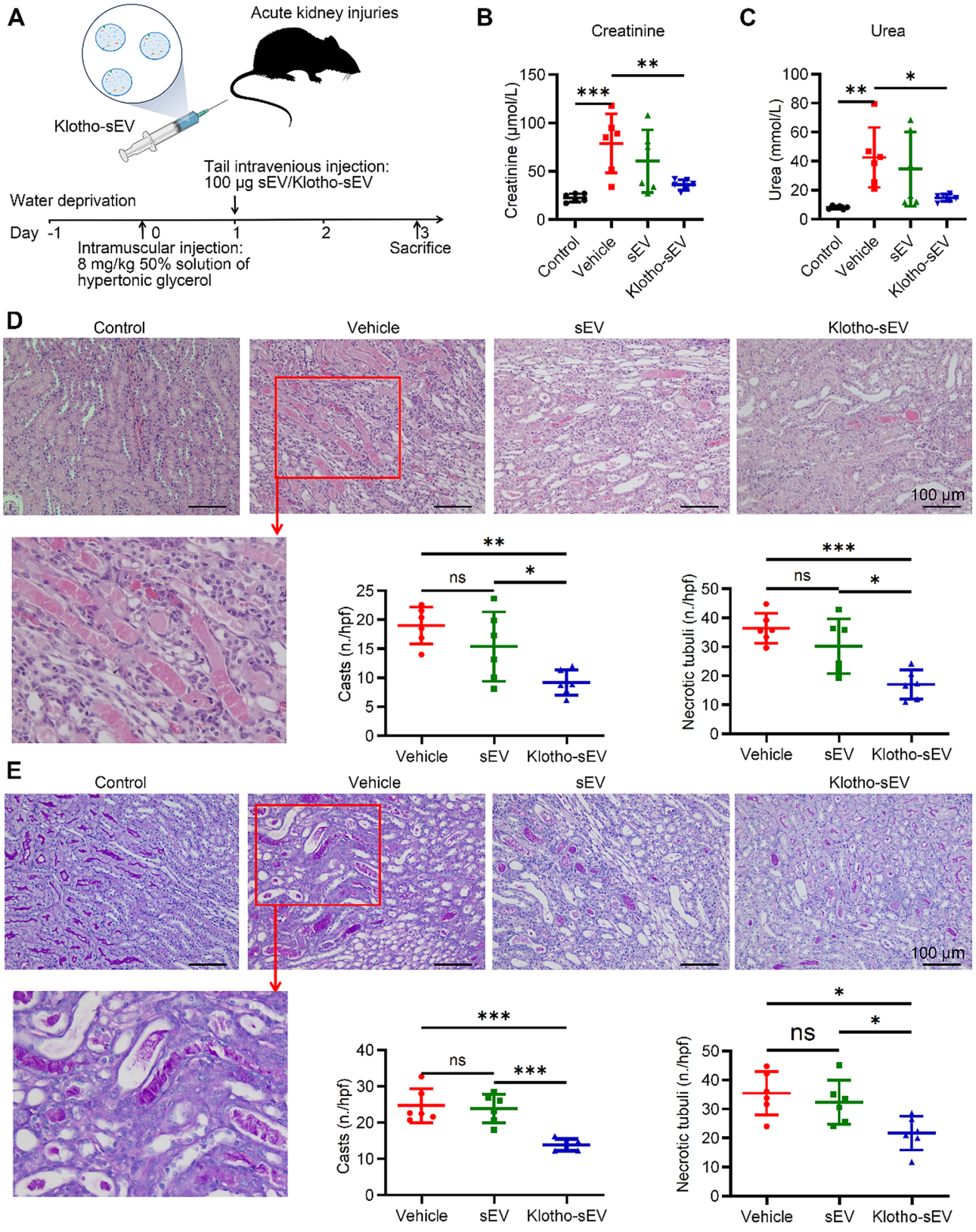

Fig. 3 (See legend on next page.)

(See figure on previous page.)

Fig. 3 Klotho-sEV significantly alleviated rhabdomyolysis-induced AKI. (**A**) Schematic of the development of rhabdomyolysis-induced AKI in mice. (**B**) Serum creatinine levels in mice subjected to different treatments. (**C**) Urea levels in the serum of mice subjected to different treatments. (**D**) Representative micrographs of hematoxylin-eosin (HE) staining of kidneys of mice with different treatments on Day 3 after damage. Original magnification ×200. (**E**) Representative micrographs of Periodic Acid-Schiff (PAS) staining of kidneys of mice with different treatments on Day 3 after damage. Original magnification ×200. In all plots, mean with SD are shown. *$p < 0.05$, **$p < 0.01$, ***$p < 0.001$, ****$p < 0.0001$ by one-way ANOVA

up-regulated expression of renal injury markers including PAI, NGAL, and SOX9. Administration of sEV slightly decreased the expression of injury markers, whereas Klotho-sEV administration significantly down-regulated the expression of these injury markers (Fig. 4B). In addition, the renal tissue of AKI mice showed a significant upregulation of pro-inflammatory cytokines including interleukin-1beta (IL-1β), IL-6 and tumor necrosis factor alpha (TNF-α). In contrast, Klotho-sEV treatment significantly reduced the expression of pro-inflammatory cytokines (Fig. 4C).

In summary, our findings demonstrated the therapeutic and regenerative effects of Klotho-sEV in rhabdomyolysis-induced AKI.

The treatment of Klotho-sEV made the proteins changed in the kidneys

To elucidate the potential molecular mechanisms of Klotho-sEV in the treatment of AKI, the total proteins were isolated from renal tissues 3 d after hypertonic glycerol treatment and subjected to 4D-DIA proteomics. A total of 10,970 proteins were identified in all the renal

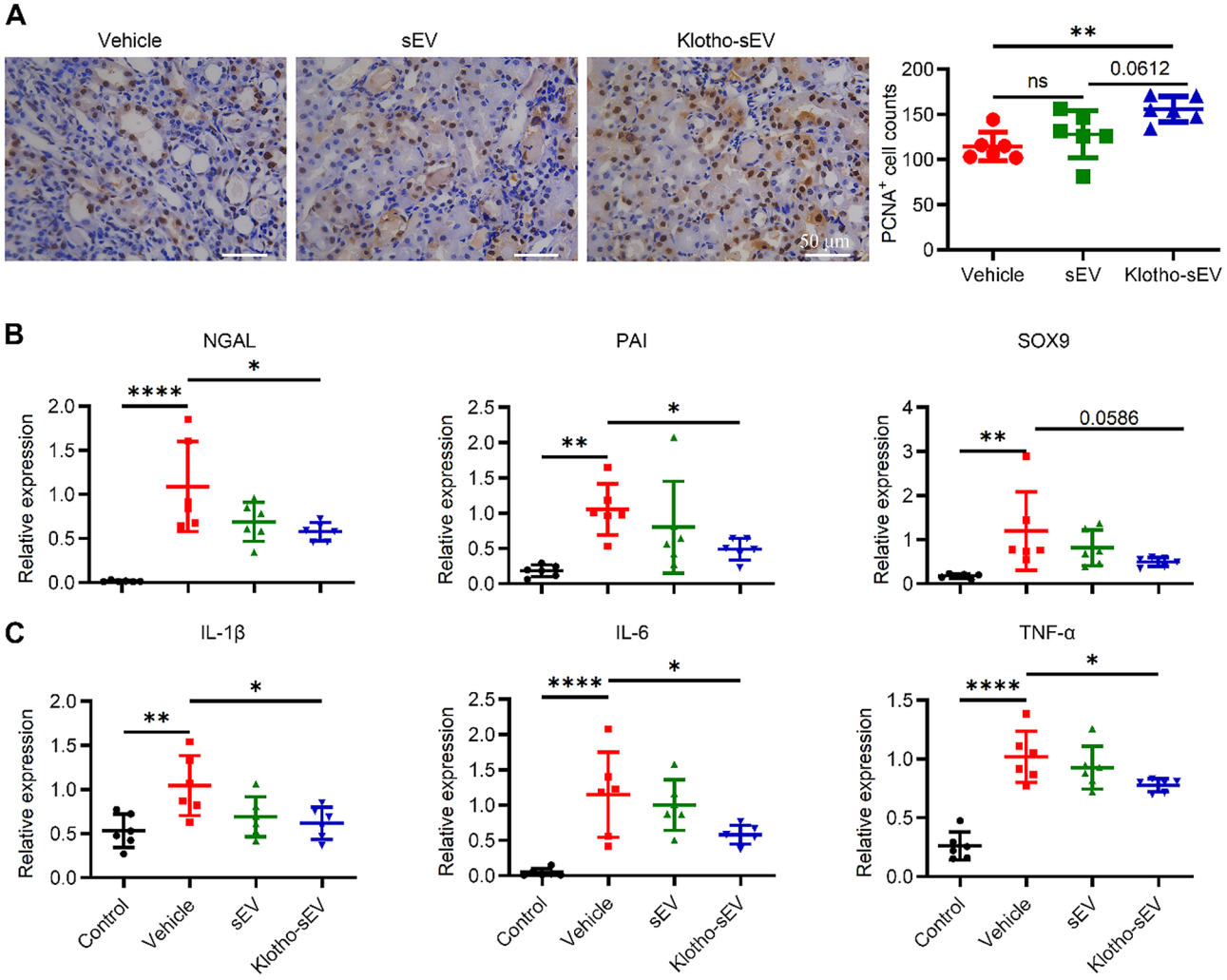

Fig. 4 Klotho-sEV significantly promoted proliferation and reduced injury and inflammatory marker expression. (**A**) Immunohistochemical staining of proliferating cell nuclear antigen (PCNA) in renal tissue. Original magnification ×400. (**B**) The mRNA levels of PAI, NGAL, SOX9 in the kidney were determined using RT-PCR. (**C**) The mRNA levels of IL-1β, IL-6, TNF-α in the kidneys were determined using RT-PCR. Means with SD are shown in all the plots. *$p < 0.05$, **$p < 0.01$, ***$p < 0.001$ by one-way ANOVA

tissues (Fig. 5A). Compared to the healthy control group, there were 1009 DEPs (296 with upregulation and 713 with downregulation) in the vehicle group, 739 DEPs (221 with upregulation and 518 with downregulation) in the sEV group, and 690 DEPs (250 with upregulation and 440 with downregulation) in the Klotho-sEV group. Compared to the vehicle group, there were 31 DEPs (11 with upregulation and 20 with downregulation) in the sEV group, 168 DEPs (132 with upregulation and 36 with downregulation) in the Klotho-sEV group. The proteins in the control group were clearly different from those in the other three groups (Vehicle, sEV, and Klotho-sEV) (Fig. 5B). DEPs in each comparison (Control vs. Vehicle, Vehicle vs. Klotho-sEV, Vehicle vs. sEV vs. Klotho-sEV, Control vs. sEV vs. Klotho-sEV) were then analyzed by hierarchical clustering, showing distinguishable (Fig. 5C-F).

We used the KEGG database to analyze DEPs in the vehicle vs. control comparison group, and the results showed that these DEPs were mainly enriched in metabolism, and metabolic pathways (295 proteins) were the most abundant. This suggests that metabolism plays a vital role in AKI. In particular, AKI had a strong impact on the PI3K-AKT, Rap1, mTOR, and PPAR signaling pathways (Fig. 5G). Further, KEGG enrichment analysis (Control vs. Vehicle vs. Klotho-sEV) showed that DEPs were mainly enriched in human diseases, organismal systems, and environmental information processing. Pathway enrichment revealed that the metabolic pathways, PI3K-AKT, Rap1, MAPK, mTOR, FoxO, and Ras pathways could participate in the disease process and repair of AKI (Fig. 5H).

Klotho-sEV treatment activated mTOR and MEK1/2 signal pathways in injured kidneys

Animal and clinical observational studies have shown that the Klotho protein not only serves as a biomarker of AKI but also functions as a promising reno-protective candidate [26, 37]. Western blotting was performed to further explore the effects of Klotho-sEV. The results showed that hypertonic glycerol treatment sharply down-regulated endogenous Klotho expression, whereas Klotho-sEV treatment reversed the levels of Klotho (Fig. 6A and B). Klotho is an essential component of endocrine fibroblast growth factor (FGF) receptor complexes as it is required for the high-affinity binding of FGF (19, 21, 23) to cognate FGF receptors [38]. mTOR and ERK1/2 are phosphorylated in the presence of Klotho and FGF [39, 40]. To validate the data from 4D-DIA proteomics and further determine the factors involved in the effects of Klotho-sEV on rhabdomyolysis-induced AKI, western blotting was performed. The pAKT levels were up-regulated after hypertonic glycerol administration (Fig. 6C). Surprisingly, we found that the phosphorylation levels of mTOR were up-regulated after Klotho-sEV treatment compared to those in the control, vehicle, and sEV groups (Fig. 6D). MEK1/2, which is upstream of ERK1/2, is involved in the MAPK pathway [41]. We found that pMEK1/2/MEK1/2 levels were dramatically down-regulated after hypertonic glycerol treatment, whereas Klotho-sEV treatment up-regulated the pMEK1/2/MEK1/2 levels (Fig. 6E).

Taken together, these data showed that Klotho-sEV restored Klotho expression in renal tissues and that the reno-protective effects of Klotho-sEV might be mediated by the phosphorylation of mTOR and MEK1/2.

sEV biodistribution and injury tropism

To elucidate the mechanisms by which sEV influence kidney function, in-vitro and in-vivo experiments were performed. Firstly, the uptake of sEV by HK2 cells was evaluated. mCherry-labelled sEV were successfully prepared (Supplementary Fig. 3A and B), and the uptake effects of HK2 cells on sEV were evaluated using flow cytometry. Using $mCherry^{+}$ cell frequencies and MFI, we observed that that sEV were significantly taken up by HK2 cells after 48 h and 72 h of incubation, and that HK2 cells took up sEV in a time-dependent manner (Fig. 7A and B). Furthermore, we confirmed the in-vitro uptake effects of HK2 cells on sEV (red) using fluorescent microscopy (Fig. 7C). These results indicate that HK2 cells took in sEV in a time-dependent manner.

Next, an endogenous labelling of sEV with a luciferase protein (NanoLuc-sEV) (Supplementary Fig. 3C-E) were used to elucidate the in-vivo distribution and tropism of sEV. Mice were injected intravenously with NanoLuc-sEV, then ex vivo imaging of the main organs was performed to determine the complete biodistribution of sEV. This analysis showed the organic distribution of sEV observed in the brains, lungs, hearts, livers, spleens, and kidneys, 1 h post-administration (Fig. 7D). For the rhabdomyolysis-induced AKI model, we observed significantly enhanced sEV accumulation in the kidneys, brains, and hearts, with most aggregation in the injured kidneys (Fig. 7D and E). Overall, these results indicate sEV preferential tropism to the injured kidneys in the setting of rhabdomyolysis-induced AKI.

Klotho-sEV and sEV contained abundant proteins

We next used iTRAQ to elucidate the protein components of Klotho-sEV and sEV. A total of 4347 proteins were identified in the two types of sEV, of which 40.9% (1776 proteins) were found in the VesiclePedia database (Fig. 8A). Conventional EV markers, CD63, CD81 and TSG101, were identified in both sEV (Supplementary Fig. 4A). Our data demonstrated that the abundance of 322 proteins (q value < 0.05) was significantly altered in the Klotho-sEV and sEV. Specifically, 212 proteins showed higher expression (Fc > 1.2), and 110 proteins

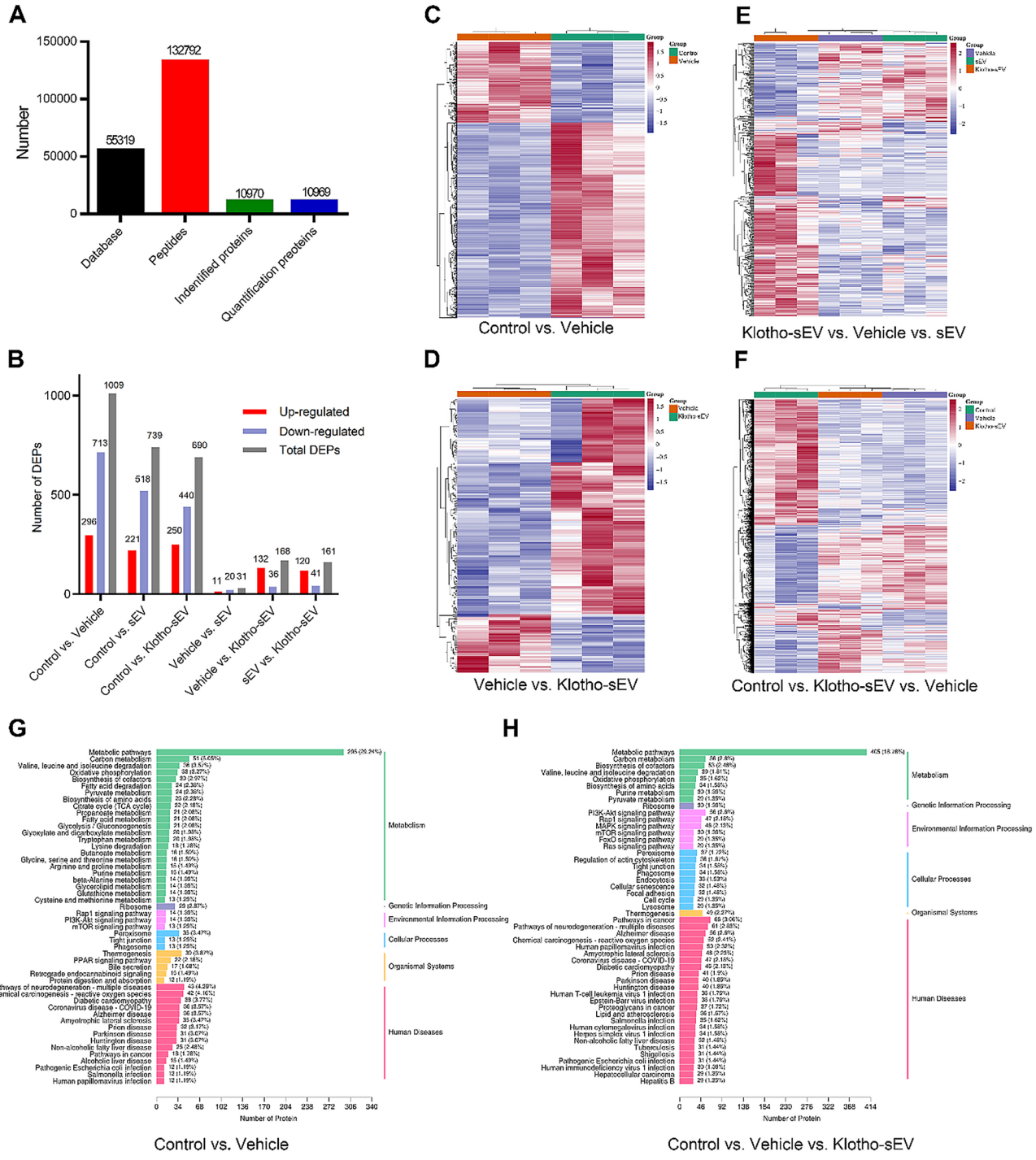

Fig. 5 Klotho-sEV treatment induced changes of proteins in AKI kidneys. Treatment with Klotho-sEV and sEV induced changes in proteins in AKI kidneys. (**A**) Identification of renal proteins by four-dimensional data-independent acquisition (4D-DIA) proteomics. (**B**) Histogram summarizing the differential expression proteins (DEPs) (fold change, Fc > 1.5 or Fc < 0.6667, and P value < 0.05) in the kidneys 3 d after hypertonic glycerol treatment. (**C**-**F**) Heatmaps showing the clustered DEPs from the comparisons of Control and Vehicle (**C**), Vehicle and Klotho-sEV (**D**), Vehicle, sEV, and Klotho-sEV (**E**), Control, Vehicle, and Klotho-sEV (**F**); the colors from blue to red indicate the expression of DEPs from low to high. (**G**-**H**) KEGG analysis from comparisons of Control and Vehicle (**G**) and Control, Vehicle, and Klotho-sEV (**H**)

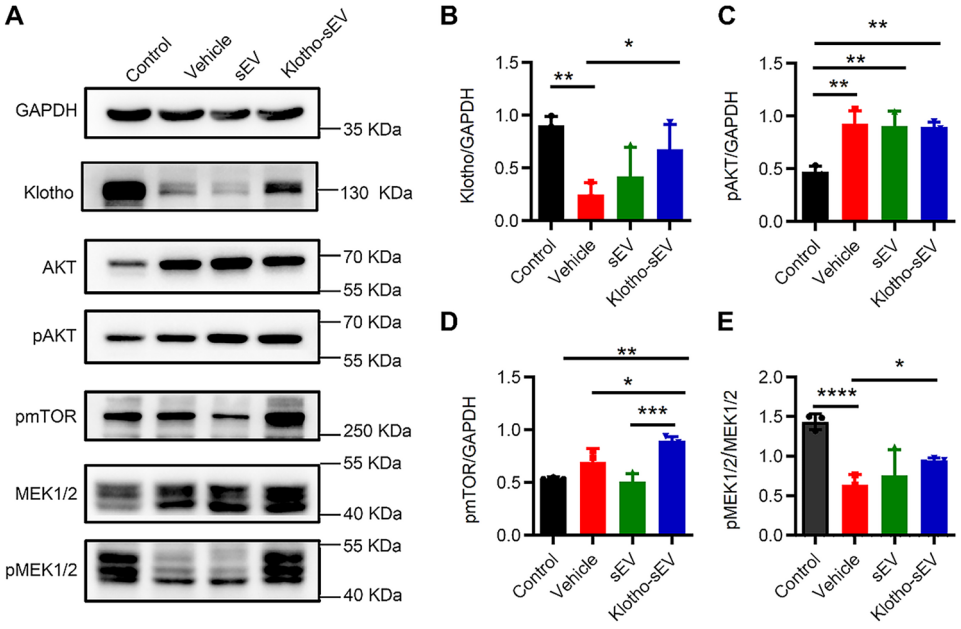

Fig. 6 mTOR and MEK1/2 phosphorylation were activated by Klotho-sEV in damaged kidneys. (**A**) GAPDH, Klotho, AKT, pAKT, pmTOR, MEK1/2, pMEK1/2 protein levels were determined using western blot. (**B**-**E**) Statistical quantification showed the relative expression of endogenous Klotho (**B**), pAKT (**C**), pmTOR (**D**), and pMEK1/2/MEK1/2 (**E**) in each group. Western blots indicated protein expression of injured kidneys in each group, 3 d after intramuscular injection of hypertonic glycerol. In all plots, mean with SD are shown. *$p < 0.05$, **$p < 0.01$, ***$p < 0.001$, ****$p < 0.0001$ by one-way ANOVA

showed lower expression (Fc < 0.8333) in Klotho-sEV than in sEV (Fig. 8B). The iTRAQ-based proteomic analysis identified 322 proteins that were categorized as cell components, the majority of which were assigned to the nucleus (114 proteins), cytosol (75 proteins), extracellular space (49 proteins), plasma membrane (32 proteins), and mitochondria (31 proteins) (Fig. 8C). Proteins with altered abundance levels were visualized in a volcano plot, which showed that most proteins were up-regulated in the Klotho-sEV (Fig. 8D). CC126, PHKG2, RMD1, LIPA3, LRP8, TPRX1, TBCA, Klotho, MYO9B, and RIPK2 were the top ten up-regulated proteins, whereas QCR1, ACSA, DKK1, PDK2, PKHA5, PEBP1, T2EA, CHID1, PTPRJ, and KCC2G were the top ten down-regulated proteins. The up-regulated expression of the Klotho protein in Klotho-sEV was confirmed. In addition, LRP8 (Fc 2.46), ARF5 (Fc 1.98), and FRAS1 (Fc 1.66) were also up-regulated (Fig. 8D and Supplementary Fig. 4B). It has been reported that LRP8, a low-density lipoprotein receptor-related protein 8, exerts anti-inflammatory activity by switching macrophages from the M1 phenotype to the M2 phenotype [42, 43]. ARF5 is a novel activator of mTOR signaling [44]; FRAS1 not only initiates kidney development but is also required for the formation of normal glomeruli [45, 46]. These data suggest that the expression of Klotho could change the protein components of sEV and that the abundant proteins in sEV might participate in reno-protection and tissue repair after injury in addition to Klotho.

We used the KOG database to analyze DEPs in the Klotho-sEV vs. sEV comparison group, and the results showed that these DEPs were mainly enriched in cellular processes and signaling, information storage and processing, and metabolism, while others were poorly characterized. Among cellular processes and signaling, signal transduction mechanisms, and post-translational modifications, protein turnover, and chaperones were the two main enriched categories. The main categories of information storage and processing were transcription, RNA processing, and modification (Fig. 8E). Furthermore, DEPs were searched in the GO database to determine enriched functional categories. According to the GO enrichment results, the DEPs of the Klotho-sEV vs. sEV comparison group were enriched in three main functional categories: biological processes, cellular components, and molecular functions. These three main functional categories were subdivided into 29, 19, and 13 smaller functional categories, respectively. Among the biological processes, cellular processes, metabolic processes, biological regulation, and regulation of biological processes were the four main enriched categories. Cells, cell parts, organelles, organelle parts, membranes, membrane-enclosed lumens, and macromolecular complexes were functional categories of DEPs that were widely enriched in the cellular components. The aggregation of DEPs in terms of molecular function was relatively concentrated primarily in terms of binding and catalytic activity (Fig. 8F). Finally, KEGG pathway analysis was performed. KEGG enrichment analysis showed

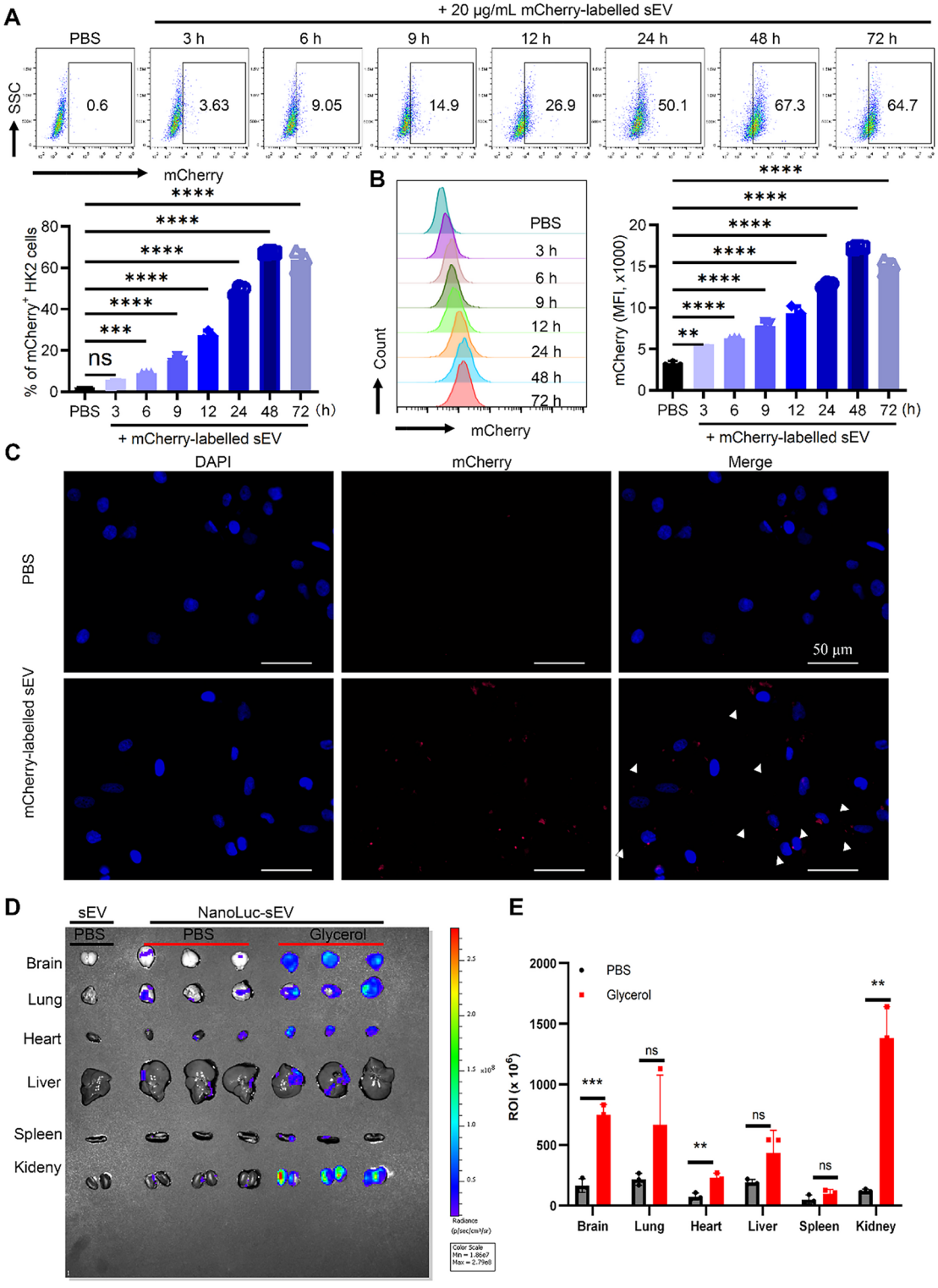

Fig. 7 Preferential tropism of sEV in damaged kidneys. (**A**) Representative flow cytometric data of human renal proximal tubule (HK2) cells incubated with mCherry-labelled sEV. The levels of mCherry positive HK2 cells were shown. (**B**) The mean fluorescence intensity (MFI) of mCherry. (**C**) Detection of mCherry in HK2 cells with mCherry-labelled sEV incubation for 24 h by means of fluorescent microscopy. Original magnification ×200. (**D**) Ex vivo imaging of the main organs from healthy mice or mice suffered from rhabdomyolysis-induced AKI. (**E**) Statistical quantification of sEV distribution in healthy mice or mice suffering from rhabdomyolysis-induced AKI. In all plots, mean with SD are shown. $^{**}p < 0.01$, $^{***}p < 0.001$, $^{****}p < 0.0001$ by unpaired t-test

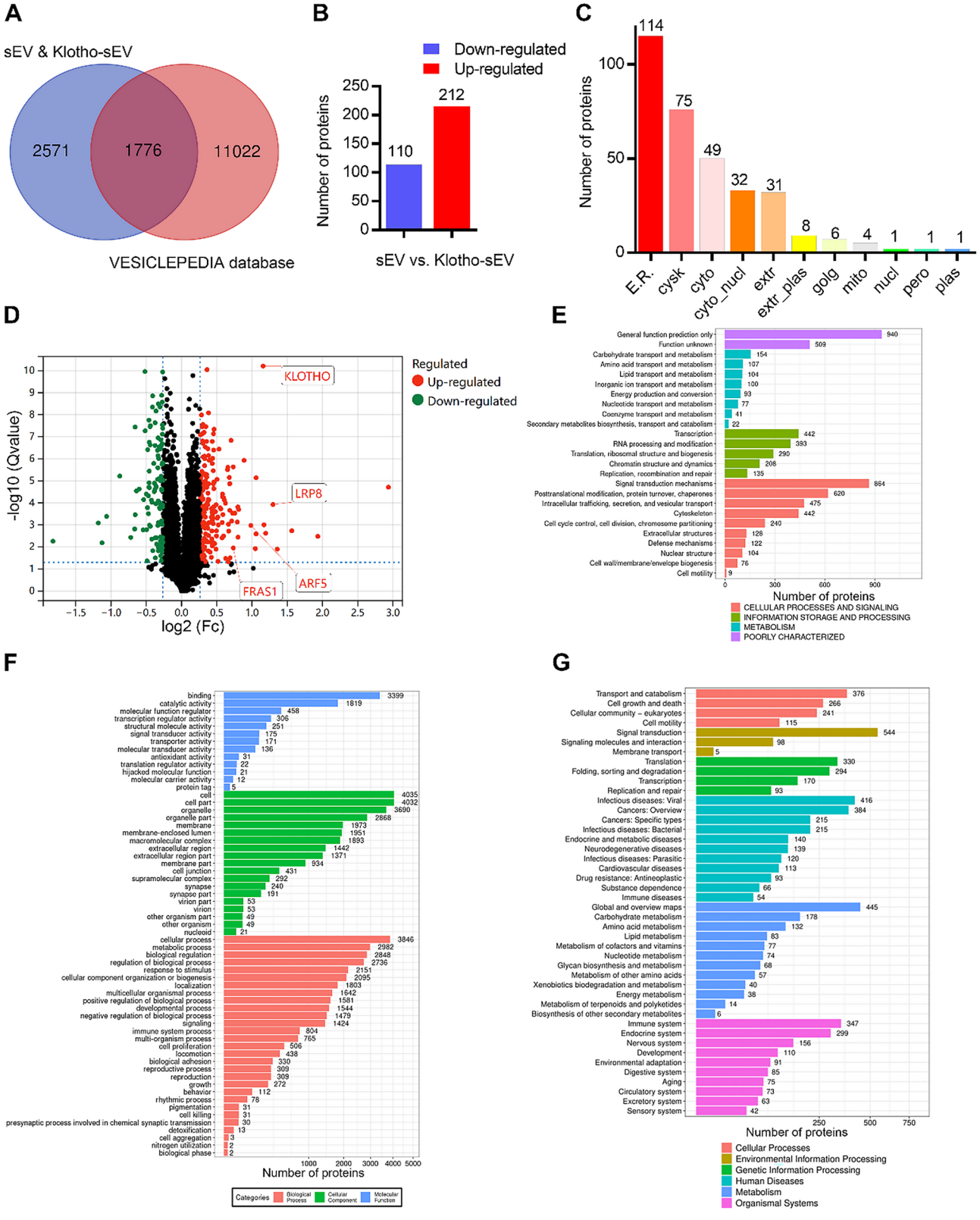

Fig. 8 sEV and Klotho-sEV were enriched in proteins. (**A**) Venn diagram of total proteins identified in sEV and Klotho-sEV compared to the VesiclePedia database. (**B**) Histogram summarizing differential expression proteins (DEPs) in sEV and Klotho-sEV (Fc > 1.2, Fc < 0.8333, and q value < 0.05). (**C**) Subcellular localization of DEPs. (**D**) Volcano plot of the proteins identified in sEV and Klotho-sEV. (**E**-**G**) KOG (**E**), GO (**F**), and KEGG pathway (**G**) analyses

that many co-differentially expressed proteins were enriched in cellular processes, environmental information processing, genetic information processing, human diseases, metabolism, and organismal systems. Cellular processes, transport and catabolism, cell growth and death, eukaryotic cellular communities, and cell mobility were the main categories. Signal transduction, signaling molecules and interactions, and membrane transport are the main categories of environmental information processing. Regarding genetic information processing, DEPs were mainly enriched in translation, folding, sorting and degradation, transcription and replication, and repair. The human disease category showed that these DEPs were mainly enriched in cancers, infectious diseases, endocrine and metabolic diseases, and neurodegenerative diseases. In addition, KEGG analysis revealed that, for metabolism, the DEPs were mainly enriched in carbohydrates, amino acids, and lipids, whereas for the organismal system, the DEPs were mainly enriched in the immune, endocrine, and nervous systems (Fig. 8G).

Overall, iTRAQ proteomics reports suggest that overexpression of Klotho by lentivirus infection could change the protein components of sEV, and other protein components in sEV might have reno-therapeutic effects in addition to Klotho.

Klotho-sEV and sEV carried abundant MiRNAs

To identify miRNA components in Klotho-sEV and sEV, we performed small RNA sequencing. A total of 1007 miRNAs were identified in Klotho-sEV and sEV, and 9 of top 10 miRNAs were common, including hsa-let-7a-5p, hsa-miR-1246, hsa-miR-146a-5p, novel-hsa-miR264-3p, hsa-let-7f-5p, hsa-let-7i-5p, hsa-miR-127-3p, hsa-miR-100-5p, and hsa-miR-181a-5p. The abundance of 51 miRNA ($|\log2Fc| \geq 0$, q value ≤ 0.05) was obviously changed in Klotho-sEV and sEV. In addition, 30 miRNAs were down-regulated in Klotho-sEV than in sEV, whereas 21 miRNAs were up-regulated in Klotho-sEV compared to sEV (Fig. 9A). Hierarchical clustering showed that the miRNAs were distinguishable between Klotho-sEV and sEV (Fig. 9B). Target prediction of differentially expressed miRNAs using GO cellular component analysis showed that most miRNAs were assigned to the cytoplasm, nucleus, cytosol, and nucleoplasm (Fig. 9C). Target prediction by KEGG pathway analysis revealed that the altered miRNAs were involved in the MAPK signaling pathway, pathways in cancer, hepatocellular carcinoma, proteoglycans in cancer, and the Rap1 signaling pathway (Fig. 9D). The miRNAs with altered abundance levels were visualized in a volcano plot, which revealed that most miRNAs were down-regulated in Klotho-sEV (Fig. 9E). hsa-miR-141-3p, hsa-miR-375-3p, novel-hsa-miR245-5p, novel-hsa-miR62-5p, hsa-miR-3651, hsa-miR-182-5p, hsa-let-7b-5p, hsa-miR-1246, novel-hsa-miR289-5p, hsa-let-7d-5p were the top 10 up-regulated miRNA, while novel-hsa-miR30-3p, novel-hsa-miR148-3p, hsa-miR-130b-5p, hsa-miR-7704, hsa-miR-487a-5p, novel-hsa-miR293-5p, hsa-miR-10a-5p, novel-hsa-miR294-3p, hsa-miR-337-5p, hsa-miR-369-3p were the top 10 down-regulated miRNAs. The let-7 family and miR-1246 exert anti-inflammatory effects [47, 48]. We found that the let-7 family (hsa-let-7a-i), miR-1246 (Fc 1.76), and miR-125b-5p (Fc 0.33) were identified in both sEV groups (Fig. 9E and Supplementary Fig. 4D), suggesting that sEV containing miRNAs might play a role in reno-protection.

Biosafety of Klotho-sEV

We further investigated the biocompatibility of Klotho-encapsulated sEV in mice (Fig. 10A). The body weights of the mice receiving different treatments were recorded every other day for two weeks. Fluctuations in the body weight of mice in each experimental group tended to be stable (Fig. 10B). In addition, there was no significant difference in blood creatinine and urea levels between the different experimental groups (Fig. 1C and D). Histological evaluation showed no evidence of detectable toxicity in the brains, hearts, lungs, livers, spleens, and kidneys (Fig. 10E). Overall, these results revealed that both sEV and Klotho-sEV were almost harmless to healthy mice.

Discussion

The global burden of AKI-related mortality remains high at 20–50%, AKI management is often suboptimal, and many cases are diagnosed late or missed entirely [2]. In the current study, we successfully developed Klotho, a reno-protective protein, encapsulated MSC-derived sEV. We demonstrated that compared to sEV, Klotho-sEV were able to stably attenuate rhabdomyolysis-induced AKI. Moreover, we revealed that Klotho-sEV exerted reno-therapeutic effects by activating the mTOR and MEK1/2 signaling pathways.

MSCs are pluripotent stem cells derived from the mesoderm that have the ability to regenerate, self-renew, and repair deficient cells. In addition, MSCs exert secretory effects that induce anti-inflammatory, immunosuppressive, and anti-fibrotic effects. Significant advances have been made in MSC transportation for various diseases such as liver disease, systemic lupus erythematosus, Crohn's disease, myocardial infarction, cerebral infarction, Parkinson's disease, and kidney disease, both in pre-clinical and clinical trials [49–53]. Although substantial evidence is available on the therapeutic effects of MSCs, their risks, including transmission of infectious factors, immune rejection, accumulation of genomic mutations and chromosomal abnormalities, and intravascular embolism, cannot be neglected [54, 55]. In recent years, it has been suggested that the therapeutic effects of

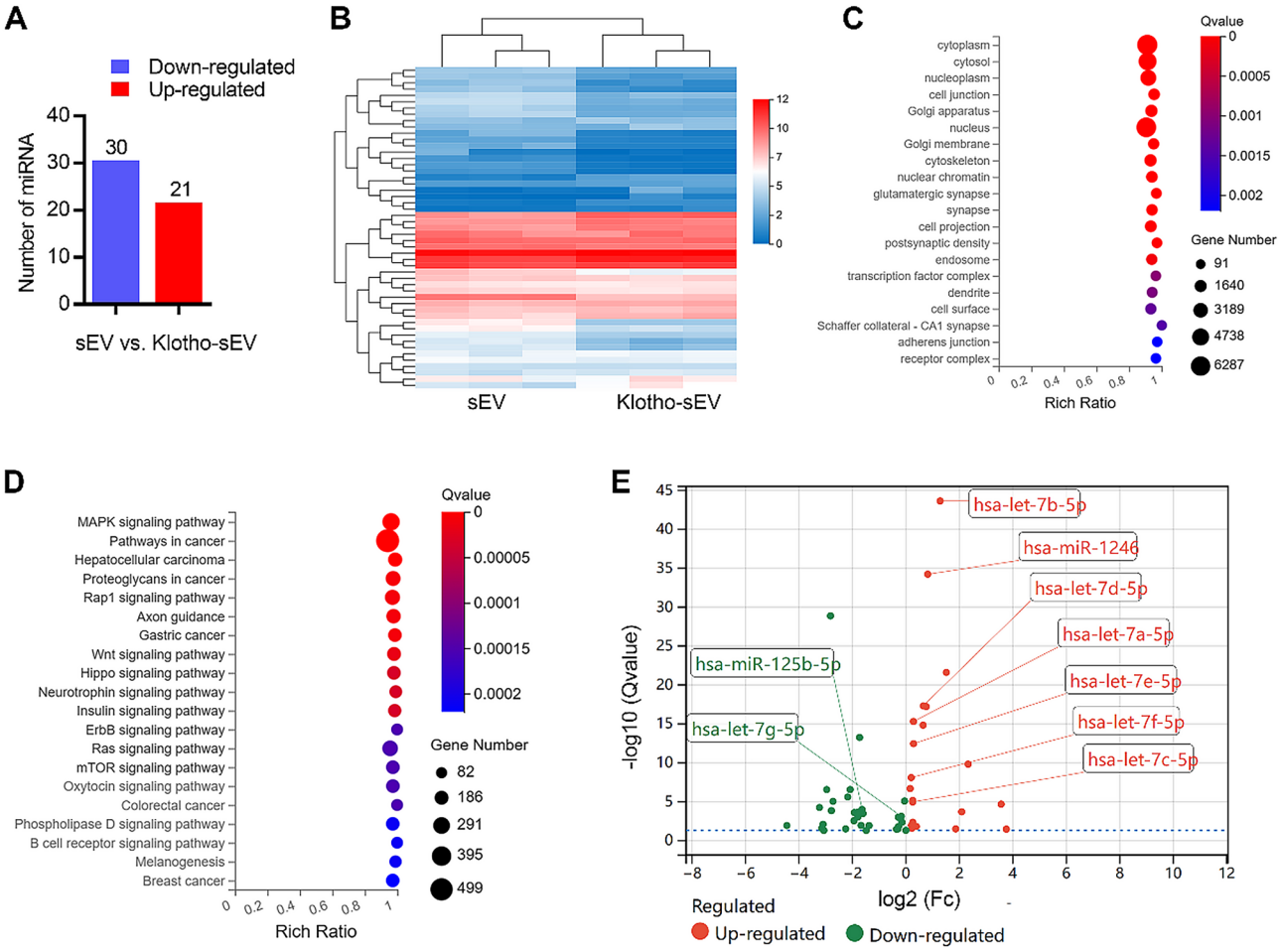

Fig. 9 Abundant miRNAs were identified in sEV and Klotho-sEV. (**A**) Differentially expressed miRNAs were shown in the histogram (|log2Fc| ≥ 0, q value ≤ 0.05). (**B**) Heat map obtained by hierarchical cluster analysis. (**C**) Target prediction of differentially expressed miRNAs using GO cellular component analysis. (**D**) Target prediction of the differentially expressed miRNAs using KEGG pathway analysis. (**E**) Volcano plot of the miRNAs identified in sEV and Klotho-sEV

MSCs are mediated by sEV secretion. MSC-derived sEV have similar therapeutic effects on MSCs because of their paracrine effects but do not have the disadvantages mentioned above [56–58]. To enhance the therapeutic effects of sEV on kidney disease, we overexpressed the renoprotective protein Klotho in MSCs by lentivirus infection to build a steady LV-KL-MSC cell line and found that approximately 74% of MSCs were infected, and Klotho overexpression did not change conventional MSC marker expression. Anion-exchange chromatography was used to isolate the sEV in the CDPF cell culture medium. Western blot, ELISA, and NanoFCM confirmed that Klotho protein was successfully loaded into the sEV and that the conventional markers of sEV were comparable in sEV and Klotho-sEV. Nanoparticle tracking analysis and transmission electron microscopy revealed that Klotho overexpression did not affect the characterization of sEV in terms of size and morphology. Previous study reported that urine derived EV contained Klotho and improved the recovery of renal function in an acute tubular injury model [20]. However, our engineered Klotho-sEV exhibited more advantages including higher Klotho levels, lower cost, easier derived and acceptable, and enhanced clinical translation potential.

AKI is a serious complication of severe rhabdomyolysis, and its prognosis is substantially worse if renal failure develops. During the Wenchuan earthquake, the mortality rate of patients with rhabdomyolysis-related AKI was 10.96% [59]. The rhabdomyolysis-induced AKI mouse model is characterized by muscle injury, the subsequent release of nephrotoxic substances, and iron deposition in the renal tissue [60, 61]. To better understand the renal absorption of sEV and sEV biodistribution in the setting of AKI, in-vitro and in-vivo experiments were conducted. We used mCherry-labelled sEV to investigate the uptake effects in HK2 cells and found that HK2 cells took in sEV in a time-dependent manner. Ex vivo imaging demonstrated that sEV were imaged in the brains, lungs, hearts,

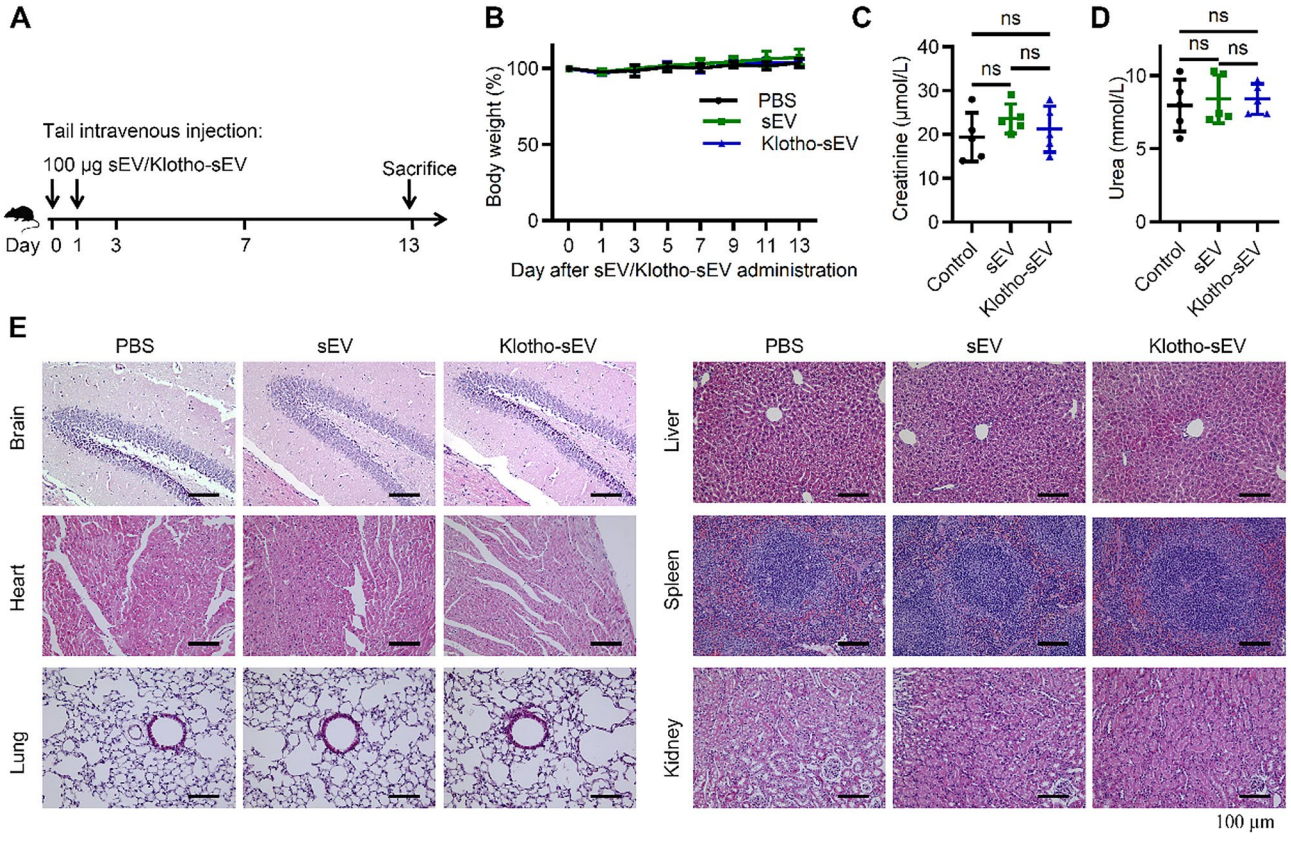

Fig. 10 In-vivo biosafety of sEV and Klotho-sEV. (**A**) Schematic for the biosafety of Klotho-sEV/sEV in mice. (**B**) Body weight of mice in different experimental groups during the treatment cycle. (**C** & **D**) The levels of creatinine (**C**) and urea (**D**) in the serum of mice treated with different agents. (**E**) Representative images of HE staining analyses to the histopathological status of the brains, hearts, lungs, livers, spleens, and kidneys of mice treated with different agents. Original magnification ×200. In all plots, mean with SD are shown. (ns, no significant, $p > 0.05$ by one-way ANOVA)

livers, spleens, and kidneys, but predominantly accumulated in the lungs. Previous studies have revealed sEV preferential tropism towards the injured kidneys [19, 20]; however, sEV biodistribution in the main organs in AKI remains to be elucidated. NanoLuc-sEV were then administered to mice 3 d after treatment with 50% solution of hypertonic glycerol by intravenous injection, and imaging was performed 1 h later. sEV showed preferential tropism to the injured kidneys, brains, and hearts and was dominantly accumulated in the injured kidneys. Therefore, our data further extend the current knowledge on the biodistribution of sEV in AKI settings.

We explored the effects of Klotho-sEV on rhabdomyolysis-induced AKI. Our in-vitro experiments showed that Klotho-sEV pretreatment ameliorated myoglobin-induced tubular cell apoptosis and increased the frequency of live cells. Moreover, in-vivo experiments demonstrated that Klotho-sEV stably accelerated renal recovery, mitigated functional and histological abnormalities, stimulated tubular cell proliferation, reduced the expression of injury and inflammatory markers, and restored endogenous Klotho loss. 4D-DIA proteomics revealed that the metabolic pathways, PI3K-AKT, Rap1, MAPK, mTOR, FoxO, and Ras pathways could participate in the disease process and repair of AKI. Western blotting confirmed that the activated AKT pathway was involved in rhabdomyolysis-induced AKI. Notably, Klotho-sEV activated the phosphorylation of mTOR and MEK1/2, consistent with previous data [39, 40, 62]. These data demonstrated that Klotho-sEV may attenuate rhabdomyolysis-induced AKI by activating the mTOR and MEK1/2 pathways.

Biological safety is essential for the clinical application of these drugs. Intravenous injection of Klotho-sEV/sEV did not cause obvious histopathological damage to the main organs, affect kidney function, or significantly alter body weight. This revealed that when used for kidney disease therapy, neither sEV nor Klotho-sEV caused adverse systemic effects.

sEV play a crucial role in the communication between cells, which relies on their cargo. In our study, 4347 proteins were identified in sEV and Klotho-sEV, of which 322 proteins were significantly altered and most DEPs were up-regulated. Subcellular location prediction of DEPs revealed that the nucleus, cytosol, and extracellular space were the major categories. A higher abundance of

Klotho in the Klotho-sEV was reconfirmed. LRP8, ARF5, and FRAS1 were also up-regulated. LRP8, low-density lipoprotein receptor-related protein 8, also named apolipoprotein E receptor-2 (apoER2) can be bind to ligand apolipoprotein E to exert its anti-inflammatory activity by switching macrophages from M1 phenotype to M2 phenotype [42, 43]. ARF5, an ADP-ribosylation factor 5, is a novel regulator of mTOR signaling [44] which may participate in the phosphorylation of mTOR in injured kidney repair. FRAS1 is a basement membrane-associated protein that mediates both the initiation of the mammalian kidney and the integrity of renal glomeruli [45, 46] which are important for maintaining renal function. These data revealed that apart from Klotho, other proteins, including but not limited to LRP8, ARF5, and FRAS1, in sEV and Klotho-sEV may exert reno-protective activity.

Much evidence has shown that nucleic acids, particularly miRNAs, a class of non-coding single-stranded RNA that exert biological functions through the post-transcriptional regulation of RNA targets, play a vital role in sEV-mediated cell-to-cell communication [63–65]. Using small RNA sequencing, 1007 miRNAs were identified of which there were 51 miRNAs that were obviously altered, and the majority of which were down-regulated. hsa-let-7a-5p, hsa-let-7f-5p, and hsa-let-7i-5p were the three most common of the top 10 abundant miRNAs in sEV and Klotho-sEV, which belong to let-7 family. In fact, let-7a-i was identified in both the sEV. The let-7 family suppresses the expression of IL-6 and IL-13, thereby participating in anti-inflammation and this has been well documented [47, 66, 67]. miR-146a inhibit inflammation and apoptosis in the diabetic retina by suppressing the IL-6-mediated STAT3/VEGF pathway [68], which was comparable in sEV and Klotho-sEV. miR-1246 (Fc 1.76) exert anti-inflammatory effects by inducing M2 macrophage polarization by targeting TER2IP via STAT3 and NF-κB pathways [48]. MSC-derived exosomal miR-125b-5p promotes tubular repair by suppressing p53 in ischemic AKI [19], in the current study, miR-125b-5p was found in both sEV and Klotho-sEV although the levels were down-regulated in Klotho-sEV. Surprisingly, Klotho mRNA accumulated in Klotho-sEV (data not shown). Sahu and colleagues demonstrated that EV from young animals rejuvenated skeletal muscle regeneration and aged cell bioenergetics in a Klotho mRNA-dependent manner [69], indicating that Klotho transcripts within sEV may contribute to the regenerative response. These data suggested that the reno-protective effects of Klotho-sEV not only rely on the Klotho protein but also some miRNAs.

Conclusion

In summary, we successfully established steady Klotho overexpressed MSCs for Klotho encapsulated sEV isolation. We found that Klotho-sEV significantly accelerated renal recovery in rhabdomyolysis-induced AKI and that Klotho mRNA, proteins, and miRNAs included in sEV may facilitate intra-nephron communication. Our study supports the further development of Klotho-sEV as an innovative cell-free therapeutic strategy for AKI treatment.

Supplementary Information

The online version contains supplementary material available at https://doi.org/10.1186/s12951-025-03499-4.

Supplementary Material 1

Supplementary Material 2

Supplementary Material 3

Supplementary Material 4

Supplementary Material 5

Supplementary Material 6

Author contributions

Xiao-Hui Deng: Writing–original draft, Software, Project administration, Methodology, Investigation, Formal analysis, Data curation, Conceptualization. Zi-Cong Wu: Project administration, Methodology, and Investigation. Qi Sun: Methodology and Formal analysis. Long-Xin Huang: Project administration, Methodology, and Investigation. Ying-Chun Xie: Project administration and Investigation. Dong-Xiao Lou: Methodology and Investigation. Chan-Gu Li: Methodology. Xiao-Qing Liu: Project administration and Investigation. Zhi-Rou Zhou: Methodology. Tian Tian: Methodology. Chang-Lin Lian: Methodology. Qing-Ling Fu: Writing–review & editing, Supervision, Methodology, Funding acquisition, Conceptualization.

Funding

This work was supported by grants from National Key R&D Program of China (2022YFA1104900), National Natural Science Foundation of China (No. 82271144 and 81970863), Guangdong Basic and Applied Basic Research Foundation (2021B1515120062), and Guangzhou Key R&D Program (2023B03J1233).

Data availability

No datasets were generated or analysed during the current study.

Declarations

Ethical approval

This study was approved by the Ethics Committee of Sun Yat-sen University (Approval number: SYSU-IACUC-2022-000827).

Competing interests

The authors declare no competing interests.

Author details

[1]Department of Otorhinolaryngology, The First Affiliated Hospital, Sun Yat-sen University, 58 Zhongshan Road II, Guangzhou 510080, Guangdong, PR China
[2]Extracellular Vesicle Research and Clinical Translational Center, The First Affiliated Hospital, Sun Yat-sen University, Guangzhou 510080, PR China
[3]Institute of Precision Medicine, The First Affiliated Hospital, Sun Yat-sen University, Guangzhou 510080, PR China

[4]Center for Stem Cell Biology and Tissue Engineering, Key Laboratory for Stem Cells and Tissue Engineering, Ministry of Education, Sun Yat-Sen University, Guangzhou 510080, Guangdong, PR China

Received: 5 February 2025 / Accepted: 27 May 2025
Published online: 07 June 2025

References

1. Menon S, Symons JM, Selewski DT. Acute Kidney Injury Pediatr Rev. 2023;44(5):265–79.
2. Kellum JA, et al. Acute kidney injury. Nat Rev Dis Primers. 2021;7(1):52.
3. Susantitaphong P, et al. World incidence of AKI: a meta-analysis. Clin J Am Soc Nephrol. 2013;8(9):1482–93.
4. Ronco C, Bellomo R, Kellum JA. Acute Kidney Injury Lancet. 2019;394(10212):1949–64.
5. Geng Y, et al. Mesenchymal stem cells ameliorate rhabdomyolysis-induced acute kidney injury via the activation of M2 macrophages. Stem Cell Res Ther. 2014;5(3):80.
6. Jiang MH, et al. Nestin(+) kidney resident mesenchymal stem cells for the treatment of acute kidney ischemia injury. Biomaterials. 2015;50:56–66.
7. Yun CW, Lee SH. Potential and therapeutic efficacy of Cell-based therapy using mesenchymal stem cells for acute/chronic kidney disease. Int J Mol Sci, 2019. 20(7).
8. Huang X, et al. Mesenchymal stem/stromal cells therapy for metabolic syndrome: potential clinical application? Stem Cells. 2023;41(10):893–906.
9. Zaripova LN et al. Mesenchymal stem cells in the pathogenesis and therapy of autoimmune and autoinflammatory diseases. Int J Mol Sci, 2023. 24(22).
10. Han Y et al. Mesenchymal stem cells for regenerative medicine. Cells, 2019. 8(8).
11. Witwer KW, et al. Defining mesenchymal stromal cell (MSC)-derived small extracellular vesicles for therapeutic applications. J Extracell Vesicles. 2019;8(1):1609206.
12. Welsh JA, et al. Minimal information for studies of extracellular vesicles (MISEV2023): from basic to advanced approaches. J Extracell Vesicles. 2024;13(2):e12404.
13. Thery C, et al. Minimal information for studies of extracellular vesicles 2018 (MISEV2018): a position statement of the international society for extracellular vesicles and update of the MISEV2014 guidelines. J Extracell Vesicles. 2018;7(1):1535750.
14. Wang X, Thomsen P. Mesenchymal stem cell-derived small extracellular vesicles and bone regeneration. Basic Clin Pharmacol Toxicol. 2021;128(1):18–36.
15. Giunti D, et al. Role of MiRNAs shuttled by mesenchymal stem cell-derived small extracellular vesicles in modulating neuroinflammation. Sci Rep. 2021;11(1):1740.
16. Woo CH, et al. Small extracellular vesicles from human adipose-derived stem cells attenuate cartilage degeneration. J Extracell Vesicles. 2020;9(1):1735249.
17. Zhou Y, et al. Exosomes released by human umbilical cord mesenchymal stem cells protect against cisplatin-induced renal oxidative stress and apoptosis in vivo and in vitro. Stem Cell Res Ther. 2013;4(2):34.
18. Wang B, et al. Pre-incubation with hucMSC-exosomes prevents cisplatin-induced nephrotoxicity by activating autophagy. Stem Cell Res Ther. 2017;8(1):75.
19. Cao JY, et al. Exosomal miR-125b-5p deriving from mesenchymal stem cells promotes tubular repair by suppression of p53 in ischemic acute kidney injury. Theranostics. 2021;11(11):5248–66.
20. Grange C, et al. Urinary extracellular vesicles carrying Klotho improve the recovery of renal function in an acute tubular injury model. Mol Ther. 2020;28(2):490–502.
21. Kuro-o M, et al. Mutation of the mouse Klotho gene leads to a syndrome resembling ageing. Nature. 1997;390(6655):45–51.
22. Wang Y, Sun Z. Current Understanding of Klotho. Ageing Res Rev. 2009;8(1):43–51.
23. Deng G, Liu D. Klotho: A promising biomarker closely related to kidney transplant. Exp Clin Transpl. 2018;16(3):253–8.
24. Hu MC, et al. Recombinant alpha-Klotho May be prophylactic and therapeutic for acute to chronic kidney disease progression and uremic cardiomyopathy. Kidney Int. 2017;91(5):1104–14.
25. Shi M, et al. AlphaKlotho mitigates progression of AKI to CKD through activation of autophagy. J Am Soc Nephrol. 2016;27(8):2331–45.
26. Hu MC, et al. Klotho deficiency is an early biomarker of renal ischemia-reperfusion injury and its replacement is protective. Kidney Int. 2010;78(12):1240–51.
27. Fang SB et al. *Small extracellular vesicles derived from human mesenchymal stromal cells prevent group 2 innate lymphoid cell-dominant allergic airway inflammation through delivery of miR-146a-5p.* J Extracell Vesicles, 2020. 9(1): p. 1723260.
28. Iwata M, Zager RA. Myoglobin inhibits proliferation of cultured human proximal tubular (HK-2) cells. Kidney Int. 1996;50(3):796–804.
29. Zhou J, et al. Myoglobin-induced apoptosis: two pathways related to Endoplasmic reticulum stress. Ther Apher Dial. 2012;16(3):272–80.
30. Bruno S, et al. Mesenchymal stem cell-derived microvesicles protect against acute tubular injury. J Am Soc Nephrol. 2009;20(5):1053–67.
31. Matsushita K, et al. Cilastatin ameliorates Rhabdomyolysis-induced AKI in mice. J Am Soc Nephrol. 2021;32(10):2579–94.
32. Komada T, et al. Role of NLRP3 inflammasomes for Rhabdomyolysis-induced acute kidney injury. Sci Rep. 2015;5:10901.
33. Reis NG, et al. Protective effect of calcitriol on rhabdomyolysis-induced acute kidney injury in rats. Sci Rep. 2019;9(1):7090.
34. Brown C, et al. Mesenchymal stem cells: cell therapy and regeneration potential. J Tissue Eng Regen Med. 2019;13(9):1738–55.
35. Zhu Y, et al. Application of mesenchymal stem cell therapy for aging frailty: from mechanisms to therapeutics. Theranostics. 2021;11(12):5675–85.
36. Li J, et al. Loganetin protects against rhabdomyolysis-induced acute kidney injury by modulating the toll-like receptor 4 signalling pathway. Br J Pharmacol. 2019;176(8):1106–21.
37. Hu MC, Moe OW. Klotho as a potential biomarker and therapy for acute kidney injury. Nat Rev Nephrol. 2012;8(7):423–9.
38. Kuro OM. The Klotho proteins in health and disease. Nat Rev Nephrol. 2019;15(1):27–44.
39. Urakawa I, et al. Klotho converts canonical FGF receptor into a specific receptor for FGF23. Nature. 2006;444(7120):770–4.
40. Benoit B, et al. Fibroblast growth factor 19 regulates skeletal muscle mass and ameliorates muscle wasting in mice. Nat Med. 2017;23(8):990–6.
41. Hendrikse CSE, et al. The potential of RAS/RAF/MEK/ERK (MAPK) signaling pathway inhibitors in ovarian cancer: A systematic review and meta-analysis. Gynecol Oncol. 2023;171:83–94.
42. Bai XQ, et al. PCSK9: A potential regulator of apoE/apoER2 against inflammation in atherosclerosis? Clin Chim Acta. 2018;483:192–6.
43. Baitsch D, et al. Apolipoprotein E induces antiinflammatory phenotype in macrophages. Arterioscler Thromb Vasc Biol. 2011;31(5):1160–8.
44. Makhoul C, et al. Arf5-mediated regulation of mTORC1 at the plasma membrane. Mol Biol Cell. 2023;34(4):ar23.
45. Vrontou S, et al. Fras1 deficiency results in cryptophthalmos, renal agenesis and blebbed phenotype in mice. Nat Genet. 2003;34(2):209–14.
46. Pitera JE, Scambler PJ, Woolf AS. Fras1, a basement membrane-associated protein mutated in Fraser syndrome, mediates both the initiation of the mammalian kidney and the integrity of renal glomeruli. Hum Mol Genet. 2008;17(24):3953–64.
47. Iliopoulos D, Hirsch HA, Struhl K. An epigenetic switch involving NF-kappaB, Lin28, Let-7 microrna, and IL6 links inflammation to cell transformation. Cell. 2009;139(4):693–706.
48. Qian M, et al. Hypoxic glioma-derived exosomes deliver microRNA-1246 to induce M2 macrophage polarization by targeting TERF2IP via the STAT3 and NF-kappaB pathways. Oncogene. 2020;39(2):428–42.
49. Li A, et al. Mesenchymal stem cell therapy: hope for patients with systemic lupus erythematosus. Front Immunol. 2021;12:728190.
50. Das M, et al. Mesenchymal stem cell therapy for the treatment of traumatic brain injury: progress and prospects. Rev Neurosci. 2019;30(8):839–55.
51. Lu M, et al. Mesenchymal stem Cell-Mediated mitochondrial transfer: a therapeutic approach for ischemic stroke. Transl Stroke Res. 2021;12(2):212–29.
52. Wang YH, Chen EQ. Mesenchymal Stem Cell Therapy Acute Liver Fail Gut Liver. 2023;17(5):674–83.
53. Gupta S, et al. Mesenchymal stem cells for cardiac regeneration: from differentiation to cell delivery. Stem Cell Rev Rep. 2021;17(5):1666–94.
54. Matsuzaka Y, Yashiro R. Therapeutic strategy of Mesenchymal-Stem-Cell-Derived extracellular vesicles as regenerative medicine. Int J Mol Sci, 2022. 23(12).
55. Yuan M, et al. Mesenchymal stem cell homing to improve therapeutic efficacy in liver disease. Stem Cell Res Ther. 2022;13(1):179.

56. Harrell CR et al. Mesenchymal stem Cell-Derived exosomes and other extracellular vesicles as new remedies in the therapy of inflammatory diseases. Cells. 2019. 8(12).
57. Torrecillas-Baena B et al. Clinical potential of mesenchymal stem Cell-Derived exosomes in bone regeneration. J Clin Med, 2023. 12(13).
58. Duong A, et al. Registered clinical trials investigating treatment with cell-derived extracellular vesicles: a scoping review. Cytotherapy. 2023;25(9):939–45.
59. Zhang L, et al. The clinical features and outcome of crush patients with acute kidney injury after the Wenchuan earthquake: differences between elderly and younger adults. Injury. 2012;43(9):1470–5.
60. Panizo N, et al. Molecular mechanisms and novel therapeutic approaches to Rhabdomyolysis-Induced acute kidney injury. Kidney Blood Press Res. 2015;40(5):520–32.
61. Safari S, et al. The value of serum creatine kinase in predicting the risk of rhabdomyolysis-induced acute kidney injury: a systematic review and meta-analysis. Clin Exp Nephrol. 2016;20(2):153–61.
62. Maekawa Y, et al. Klotho protein diminishes endothelial apoptosis and senescence via a mitogen-activated kinase pathway. Geriatr Gerontol Int. 2011;11(4):510–6.
63. Kumar MA, et al. Extracellular vesicles as tools and targets in therapy for diseases. Signal Transduct Target Ther. 2024;9(1):27.
64. Tkach M, Thery C. Communication by extracellular vesicles: where we are and where we need to go. Cell. 2016;164(6):1226–32.
65. Lu TX, Rothenberg ME. MicroRNA. J Allergy Clin Immunol. 2018;141(4):1202–7.
66. Kumar M, et al. Let-7 microRNA-mediated regulation of IL-13 and allergic airway inflammation. J Allergy Clin Immunol. 2011;128(5):1077–e851.
67. Huang Z, et al. Hsa_circ_0005519 increases IL-13/IL-6 by regulating hsa-let-7a-5p in CD4(+) T cells to affect asthma. Clin Exp Allergy. 2019;49(8):1116–27.
68. Ye EA, Steinle JJ. miR-146a suppresses STAT3/VEGF pathways and reduces apoptosis through IL-6 signaling in primary human retinal microvascular endothelial cells in high glucose conditions. Vis Res. 2017;139:15–22.
69. Sahu A, et al. Regulation of aged skeletal muscle regeneration by Circulating extracellular vesicles. Nat Aging. 2021;1(12):1148–61.

Publisher's note